Optics Letters

Ghost image restoring using random speckles created by a liquid crystal cell

Nikolay N. Davletshin,[1,2,3] Denis A. Ikonnikov,[1] Vitaly S. Sutormin,[1,2] Nikolay P. Shestakov,[1] Filipp A. Baron,[1] and Andrey M. Vyunishev[1,2,*]

[1]Kirensky Institute of Physics, Federal Research Center KSC SB RAS, Krasnoyarsk, 660036, Russia
[2]Institute of Engineering Physics and Radio Electronics, Siberian Federal University, Krasnoyarsk, 660041, Russia
[3]Federal Research Center KSC SB RAS, Krasnoyarsk, 660036, Russia
*Corresponding author: vyunishev@iph.krasn.ru

Received 13 October 2021; revised 24 November 2021; accepted 24 November 2021; posted 24 November 2021; published 16 December 2021

A liquid crystal cell is used to produce correlated light beams with speckle structures for implementation of pseudo-thermal ghost imaging. The liquid crystal cell makes it possible to provide random spatial intensity distributions, which are characterized by a low coefficient of mutual cross correlations. Ghost imaging of an object representing an amplitude mask is demonstrated. The quality of the reconstructed images was estimated by the method of structural similarity.

https://doi.org/10.1364/OL.445684

Ghost imaging (GI) is an imaging technique where the image is obtained from the spatial correlation of two light fields; one of them (object beam) interacts with an object and is measured by a single-pixel detector, whereas the other one (reference beam) is synchronously detected by a high-resolution spatial detector [1]. The idea of image restoration behind GI dates back to the seminal work by Klyshko where spatial properties of parametric downconverted photons were considered [2]. One of the first experimental confirmations of this idea was implemented on the basis of this process by Strekalov *et al.* [3]. Subsequent experiments described the GI technique as non-local quantum effects [4]. The use of the quantum concept of object image restoration using a classical light source was demonstrated by Bennink *et al.* [5]. This work is based on classical intensity correlations instead of fundamentally non-local quantum correlations, so that the main requirement for GI is a spatial correlation between the object and reference light fields. In contrast, a computational GI does not require a reference beam; however, it is necessary to know a spatial distribution of the field in the object plane [6], which requires additional complex computations. To date, there exist different modifications of GI, among them: spectral-domain [7], temporal [8], dark-field [9], and computational [6] GI. This list has recently been supplemented by ghost polarimetry [10]. The milestones and recent results in GI and single-pixel imaging are reviewed elsewhere [11].

It is well known that speckle light fields provide fascinating spatial characteristics, which are suitable for GI [12,13]. These fields are formed by mutual interference of coherent waves with random phase and/or amplitude [14]. Different diffusive elements are very attractive for producing speckle structures with random statistics and, as a result, for reconstructing the object image [11]. Among them are rotating ground glasses [12,15], liquid crystal (LC)-based spatial light modulators (SLMs) [6,16], and digital micromirror devices (DMDs) [17]. SLMs and DMDs provide a pseudo-random statistics of computer-generated speckles and they can be used as in classical and computational GI. However, high complexity, relatively low frame rate (for SLMs only), necessity for computer control, and computational effort can restrict their applications in laboratory settings. At the same time, a rotating ground glass is not capable of producing a completely random intensity distribution that does not repeat over time. Recently, continuous imaging with 1000 fps frame rate has been achieved using a 32×32 LED array illuminator [18]. In spite of this, the LED-based structured illuminators are not widespread at the moment. In contrast, LC cells have found applications in working with speckle structures. For example, a new type of speckle shearing interferometer based on the phase modulation property of a LC cell was used as a phase shifter [19,20]. The ability to control the characteristics of the LC cell makes it possible to use it in phase-only spatial light modulators [6]. On the other hand, it is possible to obtain a spatially inhomogeneous and random phase modulation of the light passing through the LC cell which is used for suppression of the speckle noise of laser radiation [21]. However, to the best of the authors' knowledge, LC cells have not been used as diffusive elements for GI.

In this letter, we consider the applicability of a single-pixel LC-based cell for producing random speckles and its implementation for restoring the image of an object using the principle of GI.

A MEST-001-13 cell (Mesostate Co., Taiwan) is used in the experiment. This cell consists of two glass substrates with transparent indium–tin–oxide (ITO) electrodes coated with alignment layers. The empty cell gap is equal to 15 μm which is filled by the LC mixture based on nematic mixture MLC-2048, 4-ethoxy-2,3-difluoro-4′-(4-pentylcyclohexyl)biphenyl and 4-methoxybenzylidene-4′-n-butylaniline. The LC has a negative value of dielectric anisotropy $\triangle\ \varepsilon = \varepsilon_{\parallel} - \varepsilon_{\perp}$, where $\varepsilon_{\parallel}$ and $\varepsilon_{\perp}$ are dielectric permittivity measured parallel and perpendicular

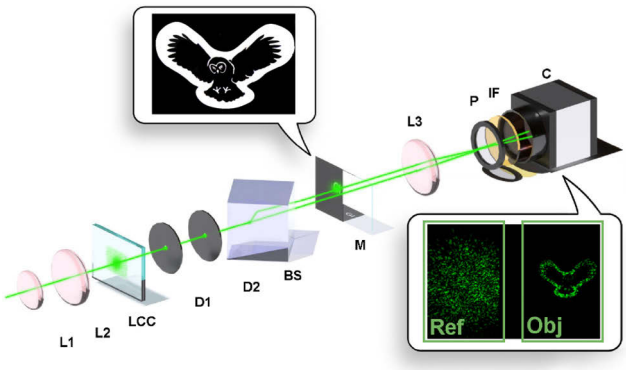

Fig. 1. Experimental setup: L1, L2, L3, lenses; LCC, liquid crystal cell; D1, D2, diaphragms; BS, beam splitter; M, object mask; P, polarizer; IF, interference filter; C, CMOS camera.

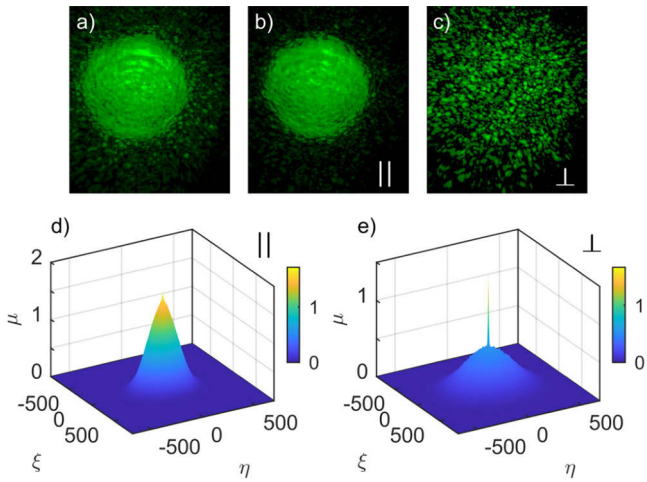

Fig. 2. Object beam cross section for various cases: non-polarized light (a), the polarizer angular position is coincident with the laser polarization (b), and polarization is orthogonal to the laser polarization (c). The AC function $\mu(\xi, \eta)$ for parallel (d) and orthogonal (e) polarizations (sample rate, 1 kHz; resolution, 1360×898 pixels; pixel sizes of CMOS, $9.6 \times 9.6\ \mu m^2$). The minimal speckle size was about 70 μm with an average of ~ 105 μm.

to the director (a unit vector characterizing the preferred orientation of the long axes of LC molecules). The generator is used for the application of electric field to the LC cell. In the absence of applied electric field, the planar director configuration (the director is oriented parallel to the cell substrates) is realized in the LC cell and the optical texture of LC layer is a homogeneous bright area. Application voltage $U = 16.6$ V at 386 Hz leads to electrohydrodynamic instability. A highly non-uniform distribution of the director is accompanied by a dynamic scattering of light. This results in random speckles of the scattered light ensured by the stochastic nature of the process.

The experimental setup is assembled by analogy with Ref. [13]. The main advantage of such a scheme is that the object and reference beams are spatially separated by two channels; after that they fall on different regions of the same camera. This ensures the synchronous detection of correlated speckles in both channels. A helium–neon laser beam of full width at half maximum of 3 mm passes through a LC cell (Fig. 1). Under certain conditions the LC cell allows scattering of the incident laser radiation into random speckles. Two diaphragms were used to control the beam size and generate speckle structures [22]. After the beam splitter, the object beam passes through an amplitude mask with image sizes 3.5×2.5 mm^2, while another one bypasses the mask. The focus lens with a focal length of 5 cm was placed after the mask to project the object and reference beams into the sensor area of a CMOS camera. The positions of the lens and camera were chosen to satisfy the criterion of classical GI restoring. Each recorded profile was divided into two different regions (frames) corresponding to separate channels (the object and reference ones, respectively). The resulting arrays were 680×898 pixels^2 per frame. A part of the sensor area corresponding to the object beam acts as a single-pixel detector in the GI restoration procedure, so the intensity is integrated over the cross section. The camera integration time was 400 μs at a speckle coherence time of about 1 ms, which ensures stable speckle structures during the measurements. The LC cell can produce speckle realizations at a frame rate up to 1 kHz, which is one order of magnitude higher than the frame rate of common SLMs. Therefore, the single-pixel LC cell can occupy an intermediate place between DMDs and SLMs by speckle pattern frame rate.

To obtain ghost images, it is important that the distribution of intensity within a cross section of the object and reference beams is random and not repeated from one realization to another. Degree of randomness of an intensity distribution over a frame can be estimated by analyzing its autocorrelation (AC) function $\mu(\xi, \eta)$, where ξ and η are array elements. The AC function of speckles is expected to have narrow strong peaks at the center in the case of absolutely random speckles. Figure 2(a) shows a typical speckle pattern produced by LC cell in the object beam. The intensity distribution is mainly uniform with small fluctuations. We revealed that the scattered light pattern depends on its polarization state. For these purposes, a polarizer was mounted before the camera. The difference between the speckle patterns for two orthogonal polarizations is evident as follows from Figs. 2(b) and 2(c) where the speckle patterns are captured with a polarizer turned parallel or perpendicular to the laser polarization. The intensity distribution corresponding to polarization normal to the laser polarization demonstrates clearly distinguishable speckle structure [Fig. 2(c)], in contrast to the case when the polarization is coincident with the laser polarization [Fig. 2(b)]. In the last case, the intensity profiles have a substrate from the laser beam incident on LC cell and as a result the respective AC function $\mu(\xi, \eta)$ is wide and smooth [Fig. 2(d)]. On the contrary, when the polarization is normal to the laser polarization, the AC function demonstrates a narrow peak corresponding to "fine structure" of speckles [Fig. 2(e)]; the width of this peak determines the correlation radius of the speckles. These results provide evidence that only part of the light is scattered by LC cell, so the residual unscattered laser radiation is still present. In the subsequent experiments, the orientation of the polarizer was set such that the polarization component coincident with the laser polarization was filtered out, leaving only good-quality speckles with orthogonal polarization suitable for GI restoration. Unfortunately, this is accompanied by remarkable intensity reduction. If the power measured before the LC cell was 0.71 mW, then after the cell (no polarizer mounted) it was 15 μW. When the polarizer was mounted, the measured powers were 8.3 μW and 4.25 μW for polarization coincident with laser polarization and orthogonal to it, respectively. Additionally to analysis

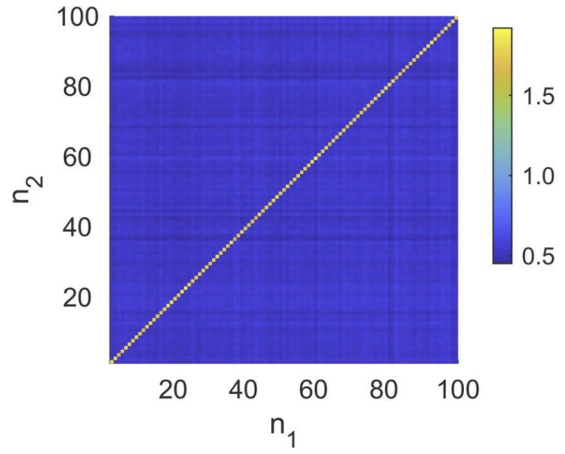

Fig. 3. Second-order intensity momentum diagram for recorded speckle realizations n_1 and n_2. Diagonal elements correspond to the AC. The contrast of the cross correlation diagram is about 4.

of the AC function of the speckle pattern in the object beam, a cross correlation function between speckle patterns in the object and reference beams was calculated. This analysis showed that these beams are spatially correlated, and, therefore, they can be used for GI restoring.

To achieve a high-quality ghost image with the minimum number of speckle realizations, it is necessary to have non-reproducibility of spatial intensity distributions. To analyze statistics of the realizations and reproducibility of intensity distributions in our optical system we recorded 300 speckle realizations of two-dimensional intensity distributions of the reference beam. Figure 3 shows the dependence of the maximum of the cross correlation function (second-order intensity momentum) in its center for a set of 100 realizations. The values of the diagonal elements are about 1.8, which is close to the theoretical value of 2 corresponding to Gaussian statistics. At the same time, the maxima of cross correlation functions of different realizations (off-diagonal elements) are close to 0.5. These characteristics are maintained for 300 speckle realizations as well. This indicates non-reproducibility of intensity distributions from one realization to another that is essential for GI restoring. The level of cross correlations suggests that the system under consideration has a high value of non-reproducibility and it is possible to use a LC cell to obtain random speckle patterns with the required spatial characteristics to restore images of an object. The probability of speckle pattern reproducibility can be less than 1/300. It is worth noting that random speckle realizations are due to dynamic scattering of light caused by the electrohydrodynamic instability of LC under alternating current. Thus, as compared to SLMs and DMDs, no additional devices are required to produce random speckle patterns by using a single-pixel LC cell.

The sample represents a glass substrate, one half of which was coated by a thin film of metal. The amplitude object mask of a *Siberian gray owl* or *phantom of the north* was imprinted on the metal film as shown in Fig. 4(a). The mask measured 3.5 mm and 2.5 mm in horizontal and vertical directions. The minimum size of individual elements of the mask was about 190μm. The full width at half maximum of the object beam was 3 mm in the object plane. The object beam spreads out when alternating current is applied to the LC cell entirely covering the mask. The

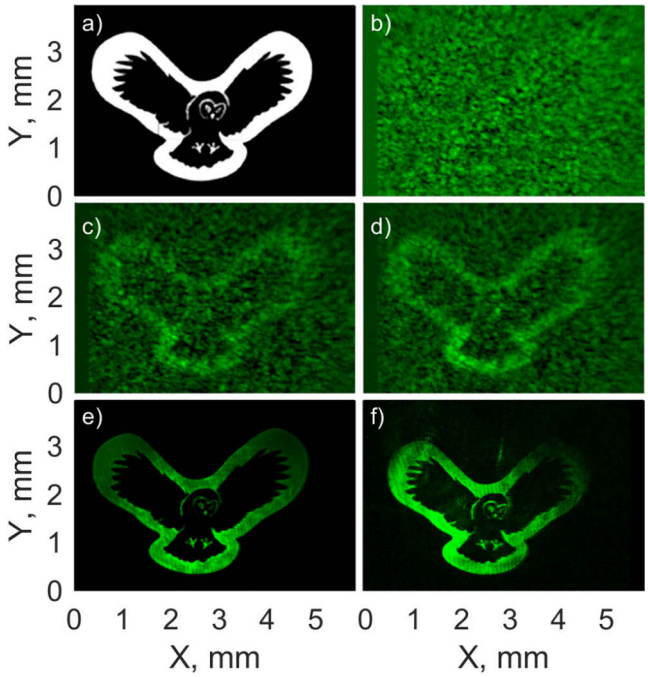

Fig. 4. Amplitude mask of a Siberian gray owl (*Strix nebulosa*) (a). The restored GI of the object mask for a number of speckle realizations of 100 (b), 2500 (c), and 5000 (d). The image of the object illuminated by speckles (averaged over 5000 realizations) (e) and the laser beam (f).

size of an individual speckle and the size of the entire speckle pattern were controlled by diaphragms D1 and D2 as shown in Fig. 1.

Both the reference and object beams were incident on the sensor area of the camera. The coefficient corresponding to the nth realization was determined as follows: $B_n = \int dxdyI_n(x, y, L)$, where $I_n(x, y, L)$ is the intensity distribution in the reference beam. The following expression was used to restore the image of the object [16]:

$$G(x, y) = \frac{1}{N}\sum_{n=1}^{N}(B_n - \langle B\rangle)I_n(x, y), \quad (1)$$

where N is the total number of speckle realizations, $\langle B\rangle$ is the average value B_n over N, and $I_n(x, y)$ is the intensity distribution in the reference beam. A total number of realizations $N = 5000$, containing complete information on both beams, was recorded. For each of the arrays corresponding to the object beam B_n, integration was performed in the image plane. Thus, for each realization, information was available about the total integrated intensity of light transmitted through the object and the spatial distribution of light in the reference beam. While the number of speckle realizations increases, the ghost image appears on the background [Figs. 4(b)–4(d)]. It is possible to distinguish a restored image of the object beginning from the 500th realization. Unfortunately, even at 5000 realizations, fine details are still not resolved [Fig. 4(d)]. Possible reasons are insufficient number of speckle realizations, mask details compared with speckles, long-range correlations [23], and the partial diffraction on the mask, which is not accounted for by the restoring procedure. In order to clarify the origin of the low degree of details, we calculated the experimental ensemble-averaged image of the object

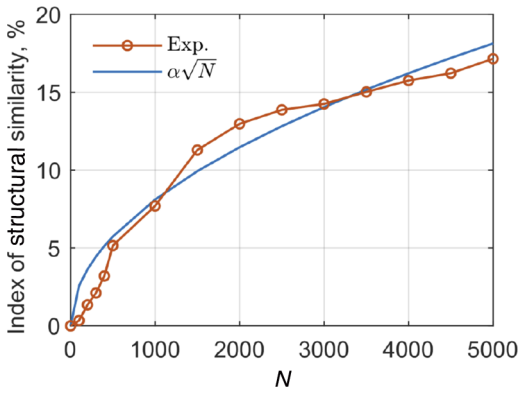

Fig. 5. Dependence of the SSIM on the number of speckle realizations N and its approximation by the function $\alpha\sqrt{N}$, where $\alpha = 0.256$.

illuminated by speckles over 5000 realizations and obtained a sharp image of the object as shown in Fig. 4(e). A similar result is obtained when the LC cell is switched off and the object is illuminated by the laser beam [Fig. 4(f)]. As is clearly seen, small details are well resolved in these cases. Thus, we assume that long-range correlations as well as diffraction do not contribute to the image restoring.

Commonly, the signal-to-noise ratio (SNR) is used to quantify the quality of ghost images. For the common case of obtaining ghost images, SNR fits well the curve $\alpha\sqrt{N}$ [13,16], assuming that the number of speckles is constant. However, the SNR does not characterize the resulting GI in terms of correspondence of the restored image to the object. To compare two images, a structural similarity index (SSIM) is widely used [24]. The SSIM allows one to estimate the similarity of two images from the point of view of human eye perception [25]. For this, the SSIM takes into account such image parameters as correlation, contrast, and brightness. The factor of correlation makes the main contribution to the SSIM. We have achieved a value of the SSIM of $\approx 17\%$ between the object mask and restored images for 5000 realizations (Fig. 5). This dependence is well approximated by the $\alpha\sqrt{N}$ curve, where N is the number of speckle realizations, so one can expect a SSIM value of 30% for 25 000 speckle realizations. Thus, there is a trade-off between the number of speckle realizations and the quality of the restored image.

In conclusion, we have demonstrated that a single-pixel LC cell operated in electrohydrodynamic instability mode is capable of producing non-repeating speckle patterns caused by dynamic scattering of light. This makes it possible to use the LC cell as the source of speckle structures for implementation of pseudo-thermal GI. A well-discerned image of an object was restored using 5000 speckle realizations. The SSIM of the restored image of 17% is achieved. Simplicity of design and fabrication, combining with simple control, make the single-pixel LC cell a good alternative to DMDs and SLMs in terms of producing random speckles ensured by the stochastic nature of the process.

Acknowledgment. The authors thank Prof. A.S. Chirkin and Prof. V.G. Arkhipkin for help and fruitful discussions and Prof. W. Lee of National Yang Ming Chiao Tung University for providing the cell used.

Disclosures. The authors declare no conflicts of interest.

Data availability. Data underlying the results presented in this paper are not publicly available at this time but may be obtained from the authors upon reasonable request.

REFERENCES

1. M. Padgett, R. Aspden, G. Gibson, M. Edgar, and G. Spalding, Opt. Photonics News **27**, 38 (2016).
2. D. Klyshko, *Photons and Nonlinear Optics* (Gordon & Breach Science, Moscow, 1988).
3. D. Strekalov, A. Sergienko, D. Klyshko, and Y. Shih, Phys. Rev. Lett. **74**, 3600 (1995).
4. T. Pittman, Y. Shih, D. Strekalov, and A. Sergienko, Phys. Rev. A **52**, R3429 (1995).
5. R. Bennink, S. Bentley, and R. Boyd, Phys. Rev. Lett. **89**, 113601 (2002).
6. J. Shapiro, Phys. Rev. A **78**, 061802 (2008).
7. C. Amiot, P. Ryczkowski, A. T. Friberg, J. M. Dudley, and G. Genty, Opt. Lett. **43**, 5025 (2018).
8. H. Wu, P. Ryczkowski, A. T. Friberg, J. M. Dudley, and G. Genty, Optica **6**, 902 (2019).
9. L.-Y. Dou, D.-Z. Cao, L. Gao, and X.-B. Song, Opt. Express **28**, 37167 (2020).
10. S. Magnitskiy, D. Agapov, and A. Chirkin, Opt. Lett. **45**, 3641 (2020).
11. G. M. Gibson, S. D. Johnson, and M. J. Padgett, Opt. Express **28**, 28190 (2020).
12. A. Gatti, E. Brambilla, M. Bache, and L. Lugiato, Phys. Rev. Lett. **93**, 093602 (2004).
13. A. Gatti, M. Bache, D. Magatti, E. Brambilla, F. Ferri, and L. Lugiato, J. Mod. Opt. **53**, 739 (2006).
14. J. Dainty, *Laser Speckle and Related Phenomena*, Vol. 9 (Springer-Verlag, 1975).
15. F. Ferri, D. Magatti, L. Lugiato, and A. Gatti, Phys. Rev. Lett. **104**, 253603 (2010).
16. Y. Bromberg, O. Katz, and Y. Silberberg, Phys. Rev. A **79**, 053840 (2009).
17. B. Sun, M. Edgar, R. Bowman, L. Vittert, S. Welsh, A. Bowman, and M. Padgett, Science **340**, 844 (2013).
18. Z.-H. Xu, W. Chen, J. Penuelas, M. Padgett, and M.-J. Sun, Opt. Express **26**, 2427 (2018).
19. H. Kadono and S. Toyooka, in *International Conference on Experimental Mechanics: Advances and Applications*, Vol. 2921, F. S. Chau and C. T. Lim, eds., International Society for Optics and Photonics (SPIE, 1997), pp. 288–293.
20. H. Kadono, S. Toyooka, and Y. Iwasaki, J. Opt. Soc. Am. A **8**, 2001 (1991).
21. A. Andreev, I. Kompanets, M. Minchenko, E. Pozhidaev, and T. Andreeva, Quantum Electron. **38**, 1166 (2008).
22. R. Meyers and K. Deacon, in *ICCES* (2007), Vol. 3, p. 211.
23. R. Berkovits and S. Feng, Phys. Rep. **238**, 135 (1994).
24. Z. Wang, A. Bovik, H. Sheikh, and E. Simoncelli, IEEE Trans. on Image Process. **13**, 600 (2004).
25. M. Sampat, Z. Wang, S. Gupta, A. Bovik, and M. Markey, IEEE Trans. on Image Process. **18**, 2385 (2009).